The correlation between aperture evolution and induced seismicity during simulated hydraulic fracturing in lab-scale coal samples

Xin Zhang
University of New South Wales, Sydney, Australia

Guangyao Si
University of New South Wales, Sydney, Australia

Joung Oh
University of New South Wales, Sydney, Australia

ABSTRACT: This paper successfully simulated the hydraulic fracturing process in lab-scale coal samples and induced seismicity using the self-developed code in particle flow code (PFC). Numerical simulations of fluid injection, fluid transport and seismic response are achieved simultaneously. The code has been applied to simulate water injection into an intact coal sample and coal samples with one pre-existing fracture. Model results satisfy observations from theoretical assumptions and laboratory experiments, which justifies the reliability of the proposed self-developed code. They indicate that hydraulic fractures on the side of the sample with a pre-existing fracture present different cracking propagation pattern compared to the other side with no pre-existing fracture. The pattern can be used to predict the impact of pre-fractures on the seismic extension-to-compression ratios and the aperture of hydraulic fractures.

Keywords: Hydraulic fracturing, Seismicity, Pre-existing fracture, Particle flow code.

1 INTRODUCTION

Hydraulic fracturing is widely used in the energy resource sector, not only to enhance oil and gas production in tight reservoirs but also to facilitate caving and prevent dynamic disasters in mining (Huang & Liu 2017). However, due to the geological complexities, although there are novel failure mechanism theories (Fischer & Guest 2011), it is still challenging to determine the in-situ conditions for various modes of rock failure at target depths and fluid pressure regimes in a reservoir. Seismic monitoring is an important tool to infer subsurface rock failure behaviour reservoir properties (e.g., stress, permeability, connectivity) adjacent to induced fractures (Rutledge et al. 2004 and Guo et al. 2021). However, the conclusions drawn cannot be easily validated and widely transferred due to the geological complexity and uniqueness of specific regions.

Numerical modelling has provided a unique strength to simulate rock failure under various stress and geological conditions. The discrete element method (DEM) has become increasingly popular in recent years because it allows a better understanding of crack initiation and growth in rocks with pre-fractures or flaws (Potyondy 2010). In addition, a systematic set of methods and theories have been proposed in DEM to not only numerically reproduce seismicity but also to model the seismicity

induced by fluid injection in naturally fractured rocks (Hazzard & Young 2000 and Al-Busaidi et al. 2005). For instance, Zhao & Young (2011) simulated fluid injection via PFC to study different modes of interaction between pre-fractures of different orientations and hydraulic fractures under various stress boundaries. The corresponding seismic events and their moment tensors were calculated and visualised on simulated rock samples.

However, seismic responses produced in hydraulic fracturing simulations have been rarely used to invert rock behaviours and property changes. There is limited research to apply advanced analysis to understand the relationships between the rock failure behaviour and related seismicity. For instance, seismic data are used to deduce the aperture of hydraulic fractures in the field, but these hypotheses have not been widely tested via numerical simulation. In addition, hydraulic fracturing and seismic monitoring targeted at coal seams are becoming increasingly popular since fluid injection is more frequently employed to fracture the coal seam near mining face worldwide (Hu et al. 2020). However, there are limited studies on simulating hydraulic fracturing in coal samples and considering seismic responses. This paper examines the feasibility of using PFC to simulate fluid injection and induced seismicity in lab-scale coal samples. It then analyses the evolution of simulated acoustic emission (AE) events and moment tensors to understand how they correlate to the aperture of hydraulic fractures.

2 METHODOLOGY DEVELOPMENT AND CALIBRATION

The simulation of hydraulic fracturing is conducted by the PFC2D (Itasca 2008). The self-developed hydraulic fracturing module and seismic simulation module in PFC can be integrated in tree steps: to calibrate the simulated rock sample, to construct the flow domain network in the target cubic sample, and finally to apply boundary condition to reach the initial model equilibrium before injection. The realization of fluid injection includes three parts: construction of domain skeleton, definition of fluid flow and fluid pressure updates and coupling with the particles and contacts (Al-Busaidi et al. 2005 and Zhang et al. 2021). Once the injection begins, the pore pressure in fluid domains is calculated which is then coupled with the principal stress and particle bond stress to calculate the effective stress. At the same time, the module to simulate the triggering of AE events is executed independently at every timestep to detect the failure among bond contacts and calculate the associated seismic moment tensors. In this model the moment tensor is calculated crack geometry and force-displacement relations (Aki & Richards 1980).

The proposed model is well calibrated to achieve reasonable mechanical responses that are compatible with the laboratory observations in terms of stress-strain curve and Poisson's ratio. The calibrated input parameters for the model are determined by Zhang et al. (2023). In numerical modelling, injection with constant pressure is preferred compared to the constant flow rate because of its capability to keep a stable fluid flow, especially in 2D models (Al-Busaidi et al. 2005). Table 1 includes the key injection parameters refined from the lab experiments and previous modelling practices (Zhang 2019 and Zhang et al. 2021).

Table 1. Input micro parameters in PFC for model calibration.

Model input parameter	Symbol	Value
Fluid injection		
Borehole radius, mm	r	2
Injection pressure, MPa	P_{inj}	5
Vertical compressive stress, MPa	σ_1	4
Horizontal compressive stress, MPa	σ_3	2
Initial hydraulic aperture, mm	e_0	0.5
Infinite hydraulic aperture, mm	$e_{\inf}$	0.05
Fluid dynamic viscosity, Pa•s	η	1e-3
Bulk modulus of fluid, GPa	K_f	2.2
Pre-fracture		

Length, mm	L	40
Width, mm	W	2
Orientation	θ	0^0
Tensile strength, MPa	σ_t	0.1
Cohesion, MPa	c	0.3

After the calibration, several scenarios are set up to further test the reliability of the injection model. Case 1 is designed as only the intact rock sample, and its geometry and boundary conditions are shown in Figure 1 (a). Building upon Case 1, Case 2 considers one fracture 40 mm long at the upper part of the sample as shown in Figure 1 (b). The smooth joint contact model is selected here to model the pre-existing fracture (or pre-fracture) (Mars 2010), while particles in the rest of the sample are bonded by the linear parallel bond contact model (Potyondy & Cundall 2004). For comparison purposes, in Case 3, another single fracture with the same property is defined at the lower part of the sample as shown in Figure 1 (c), which mirrors that in Case 2. All the pre-existing fractures have the same length since the length is not the research focus here although it can affect fracturing behaviours. All cases share the same input parameters as given in Table 1.

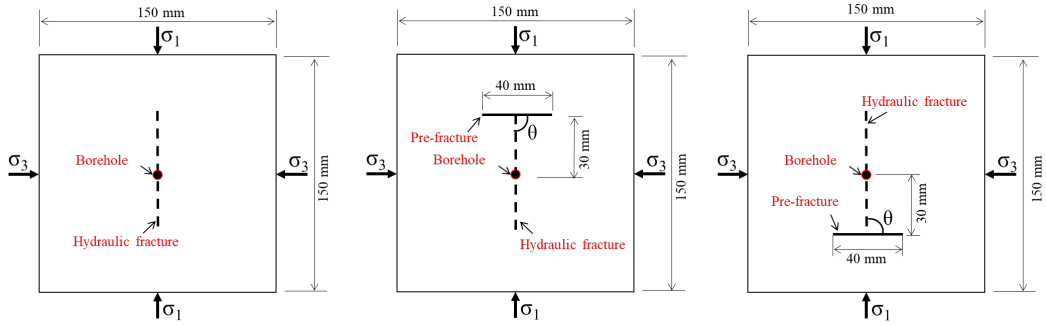

(a) (b) (c)

Figure 1. Geometry of the simulated coal samples: (a) Case 1: intact coal sample, (b) Case 2: single upper fracture, and (c) Case 3: single lower fracture.

3 MODEL RESULTS AND DISCUSSIONS

3.1 Evolution of simulated AE events and moment tensors

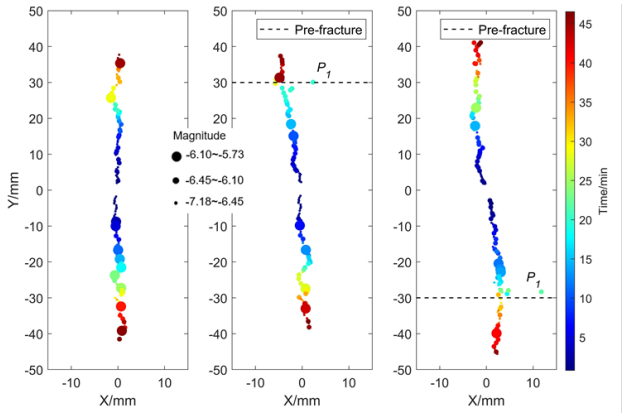

(a) (b) (c)

Figure 2. Spatial distribution of AE events: (a) Case 1: intact sample; (b) Case 2: single upper fracture; (c) Case 3: single lower fracture.

The spatial evolution of AE events is shown in Figure 2. For better visualisation only the central part of the simulated coal sample is shown here because there are no AE events recorded outside this area. Samples are cracked after 47 minutes producing around 120 seismic events. The colourmap shows the event triggering time and the colour-coded data points are marked by different sizes to represent event magnitude. The overall spatial distribution of AE events is propagating from the borehole towards the top and bottom boundaries, roughly following the maximum principal stress direction especially for Case 1 in Figure 2 (a). The resultant formation of hydraulic fractures is defined as 'cross', referring to the hydraulic fractures which run through the pre-fracture parallel to the minimum principal stress direction (Zhao & Young 2011).

In Case 2 and Case 3, the trajectory of AE event propagation deviated away from the maximum principal stress before coming across the pre-fracture. What's more, there are a couple of AE events inside the pre-fracture but at a short distance away from the overall trajectory. According to its triggering time, the event, marked as P_1, is essentially the earliest event when the cracking front is approaching the pre-fracture which can be reasonably treated as induced seismicity. To emphasize the difference exposed by the pre-fracture, only Case 2 and Case 3 are compared in following sections.

The distance between the borehole centre and AE events triggered at different times is presented for the upper and lower trajectories, as depicted by red and black curves in Figure 3, respectively. In addition, the propagation distance difference between two directions is computed for better comparison, which is shown by the blue bar chart. For Case 2 shown in Figure 3 (a), although the crack propagation rates are similar at the beginning, after about 10 mm from the borehole on the y-axis, AE events in the upper part of the coal sample were recorded earlier than their counterparts in the lower section, given the same distance from the borehole. This difference in the crack growth rate lasts for a while until AE events reach the pre-fracture position (y=30 mm). In terms of the travelling velocity, the propagation of hydraulic fractures from both sides can be divided into three stages by two typical time points (T_1 and T_2) from Figure 3 (a). At 21.6 minutes, the distance difference has reached the peak value of 9 mm at the deviation point P_1, which is also the earliest AE event reported near the pre-fracture. In Figure 3 (b), model results in Case 3 show similar observations as that in Case 2 but in an opposite direction. It also has a very similar three-stage behaviour in terms of the crack propagation distance difference, which is restrained by T'_1 and T'_2, and the peak value of the distance difference is marked by P_1.

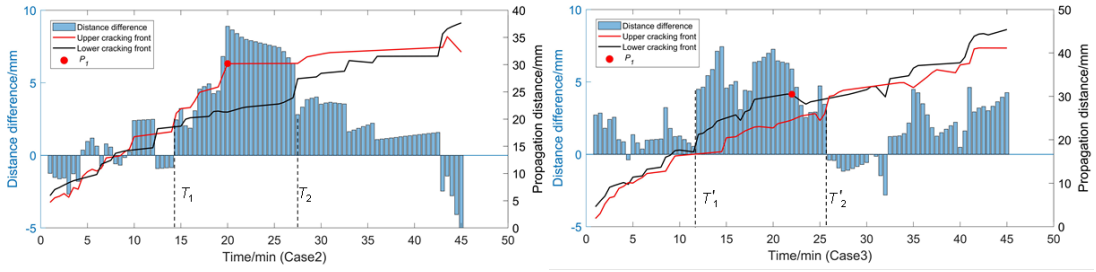

(a) (b)

Figure 3. Distance between the upper/lower cracking fronts and the borehole centre: (a) Case 2; (b) Case 3.

To study the failure mechanism during the fluid injection, the principal directions of moment tensors for AE events can also be calculated to describe the orientation of individual hydraulic fractures. Every eigenvector has a long axis and a short axis, which are orthogonal to each other and represent the major and minor principal directions, respectively (Hazzard & Young 2002). Thus, for a tensile crack, the short axis indicating compression normally points inward to the crack centre. To assess the percentage of the extension component in an AE event, the extension-to-compression ratio is defined here, which is measured by the ratio of the long axis to the short axis. From Figure 4, the extension components have overwhelming magnitude over compression, with most ratios falling between 1 and 20. The ratios in Case 2 have most of the peaks from T_1 to T_2, as shown in Figure 4 (a). Similarly, Case 3 also has most of the ratio peaks during the period of propagation distance difference between by T'_1 and T'_2, as shown in Figure 4 (b). Most of the ratio values and peaks are focused within the distance difference area. Thus, the variation of extension-to-compression ratios

seems to be correlated with the period with a large difference in crack propagation distance, which is apparently affected by the pre-fractures.

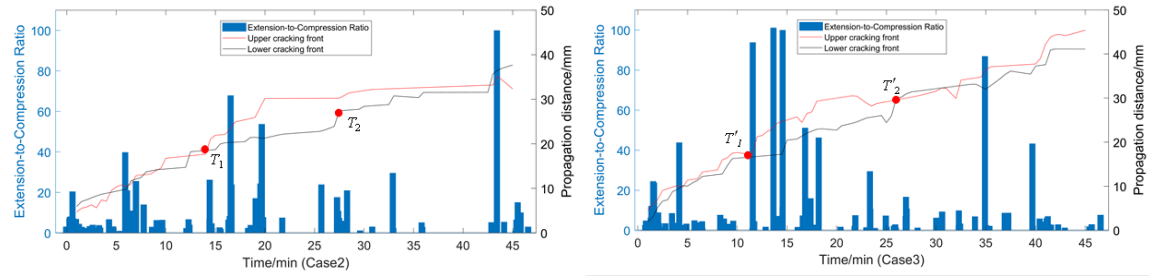

(a) (b)

Figure 4. Ratio of the long axis to the short axis of decomposed seismic moment tensors: (a) Case 2: intact sample and (b) Case 3: single upper fracture.

3.2 Correlated apertures of hydraulic fractures with seismicity

The deformation and displacement of rock particles are related to the aperture of the domain structure, which directly affects the conductivity of fractures. To assess how the aperture can change dynamically with the propagation of hydraulic fractures, two measurement points are assigned near the injection borehole as shown in Figure 5 (a).

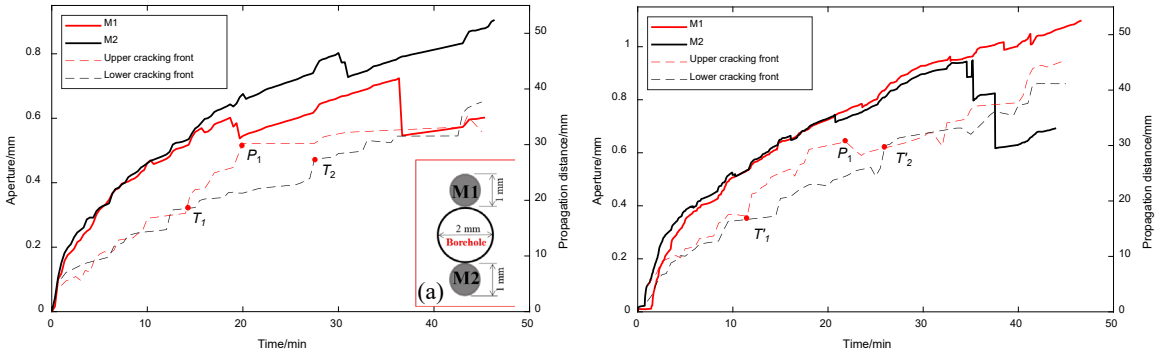

(b) (c)

Figure 5. (a) Assignment of two measurement points near the injection borehole; evolution of the aperture within the measurement circles during fluid injection for (b) Case 2 (c) Case 3.

Figure 5 (b) shows the average aperture of all flow channels within the defined measurement points (M1 and M2). In Case 2, the aperture in M1, which is on the upper part with the pre-fracture, experiences two large drops. The first aperture drop happens near P_1 during the notable distance difference from 0.61 mm to 0.53 mm. The second drop at 35 minutes happens after hydraulic fractures completely cross the pre-fracture. The average aperture within M2 has a relatively more linear increase from 0 mm to 0.91 mm, except for a mild drop at around 30 minutes. Therefore, the presence of the pre-fracture suppresses the aperture growth, and this effect can be implied by the early deviation of AE events. Similar model results in Case 3 are presented in Figure 5 (c). The aperture difference can also be observed after point P_1, when the cracking front distance difference is the largest. The average aperture within M2 also has a dramatic drop after hydraulic fractures pass through the pre-fracture.

4 CONCLUSIONS

Hydraulic fracturing has been successfully simulated using PFC2D to investigate rock failure behaviour and related seismicity in lab-scale coal samples with single pre-existing fractures. In flow domain structures, constructed based on bonded particles, the flow pressure is updated using the injection algorithm modified from Darcy's law. Meanwhile, seismic activities induced by fluid injection can be simulated by calculating moment tensors using force-displacement relations.

The simulated seismicity shows that the pre-fracture can cause a notable distance difference in the cracking front: AE events on the side with the pre-fracture will propagate much faster when approaching the pre-fracture. Over the same period designated by the notable distance difference, there are more peak values of extension-to-compression ratios, would be observed. Meanwhile, the aperture of hydraulic fractures on the side of the pre-fracture will become smaller than that on the opposite side.

REFERENCES

Aki, K. & Richards, P.G. 1980. *Quantitative Seismology*. Freeman, New York.

Al-Busaidi, A., Hazzard, J.F. & Young, R.P. 2005. Distinct element modelling of hydraulically fractured Lac du Bonnet granite. *Journal of Geophysical Research* 110, pp. B06302.

Bowers, D. & Hudson, J.A. 1999. Defining the scalar moment of a seismic source with a general moment tensor. *Bulletin of the Seismological Society of America* 89, pp. 1390-1394.

Fischer, T. & Guest A. 2011. Shear and tensile earthquakes caused by fluid injection. *Geophysical Research Letters* 38, pp. L05307. Doi:10.1029/2010GL045447

Guo, H., McGuire, J.J. & Zhang, H. 2021. Correlation of porosity variations and rheological transitions on the southern Cascadia megathrust. *Nature Geoscience* 14, pp. 341-348.

Hazzard, J.F. & Young, R.P. 2000. Simulating acoustic emissions in bonded-particle models of rock. *International Journal of Rock Mechanics and Mining Sciences* 37, pp. 867-872.

Hazzard, J.F. & Young, R.P. 2002. Moment tensors and micromechanical models. *Tectonophysics* 356, pp.181-197. Doi: https://doi.org/10.1016/S0040-1951(02)00384-0

Hu, Q., Liu, L., Li, Q., Wu, Y., Wang X., Jiang, Z., Yan F., Xu Y. & Wu X. 2020. Experimental investigation on crack competitive extension during hydraulic fracturing in coal measures strata. *Fuel* 265, pp. 117003.

Huang, B. & Liu, J. 2017. Experimental investigation of the effect of bedding planes on hydraulic fracturing under true triaxial stress. Rock Mechanics and Rock Engineering 50, pp. 2627-2643.

ITASCA Consulting Group Inc. 2008. *PFC2D-Particle Flow Code in 2 Dimensions (Version 4.0)*, Minneapolis. Itasca Consulting Group Inc. 2008. Technical Memorandum-5.0 Parallel Bond Enhancement.

Mars Ivars, D. 2010. *Bonded particle model for jointed rock mass*. Department of Land and Water Resources Engineering, Royal Institute of Technology (KTH), Stockholm, Sweden.

Potyondy, D.O. 2010. A grain-based model for rock: approaching the true microstructure. In: *Proceedings of Rock Mechanics in the Nordic Countries 2010 (Bergmekanikki Norden 2010)*, Kongsberg, Norway, 9-12 June.

Rutledge, J.T., Phillips, W.S. & Mayerhofer, M.J. 2004. Faulting induced by forced fluid injection and fluid flow forced by faulting: an interpretation of hydraulic fracture microseismicity, Carthage Cotton Valley gas field, Texas. *Bulletin of the Seismological Society of America* 94, pp.1817-1830.

Zhang, R., Zhao, C., Yang, C., Xing, J. & Morita, C. 2021. A comprehensive study of single-flawed granite hydraulically fracturing with laboratory experiments and flat-jointed bonded particle modeling. *Computers and Geotechnics* 140, pp.104440. Doi: https://doi.org/10.1016/j.compgeo.2021.104440

Zhang, X. 2019. Characteristics of hydraulic fracturing induced AE signals and fracture localization. China University of Mining and Technology. Xuzhou, China.

Zhao, X.P. & Young P.R. 2011. Numerical modelling of seismicity induced by fluid injection in naturally fractured reservoirs. *Geophysics* 76, pp. WC167-WC180. Doi: https://doi.org/10.1190/geo2011-0025.1.

Zhang, X., Si, G., Bai, Q., Xiang, Z., Li, X., Oh, J. & Zhang, Z. 2023. Numerical simulation of hydraulic fracturing and associated seismicity in lab-scale coal samples: A new insight into the stress and aperture evolution. *Computers and Geotechnics* 160, 105507. Doi: https://doi.org/10.1016/j.compgeo.2023.105507.